



# Light-patterned fluorescent gold nanoclusters in polycarbonate films

MOHAMMAD H. BITARAFAN,<sup>1,\*</sup> SHAOCHEN ZHOU,<sup>2</sup> JUSSI HÄNNINEN,<sup>1</sup> YANYAN DUAN,<sup>3</sup> MARTTI LEINO,<sup>1</sup> ROBIN H. A. RAS,<sup>2,4</sup> AND JUHA TOIVONEN<sup>1</sup> 

<sup>1</sup>Photonics Laboratory, Physics Unit, Tampere University, Korkeakoulunkatu 3, FI-33720 Tampere, Finland

<sup>2</sup>Department of Applied Physics, Aalto University School of Science, Puumiehenkuja 2, FI-00076 Espoo, Finland

<sup>3</sup>IMDEA Materials Institute, Calle Eric Kandel 2, 28906 Getafe, Spain

<sup>4</sup>Department of Bioproducts and Biosystems, Aalto University School of Chemical Engineering, P.O. Box 16000, FI-00076 Espoo, Finland

\*mohammad.bitarafan@tuni.fi

**Abstract:** Fluorescent metal nanoclusters embedded in rigid matrices are attractive for many applications, such as for use as light-emitting diodes and for optical data storage. Given the advantages of polycarbonate films, like high transparency and excellent toughness, the development of metal nanoclusters in these films could further enhance various applications. Herein, we fabricated fluorescent gold nanoclusters in a polycarbonate film using a photochemical process. The polymer film is doped with gold chloride and a photoinitiator and then irradiated by a light-emitting diode (365 nm), leading to the photoreduction of gold ions and the formation of bright fluorescent nanoclusters with a quantum yield of 15%. The as-formed nanoclusters display good photostability and retain their emission spectral shape over an extended period of time. These highly fluorescent structures have potential applications in the fabrication of authenticity markings and optoelectronic devices.

© 2021 Optica Publishing Group under the terms of the [Optica Open Access Publishing Agreement](#)

## 1. Introduction

Metal nanoclusters (NCs) are ensembles of bound metal atoms that are intermediate in size between single metal atoms and plasmonic nanoparticles (NPs)—i.e., below 2 nm in diameter [1–3], exhibiting quasi-molecule behaviors such as strong absorption and intense photoluminescence (PL) [4,5]. Given the ultra-small size, low toxicity, large Stokes shift, long lifetime, and good photostability, NCs find various applications, including sensing, labeling, and imaging [3,5–8]. The synthesis of NCs is a major issue and the subject of interdisciplinary research from chemistry to photonics. A well-known approach to produce NCs is reducing metal ions (using, for example, chemical reductants or light) from dissolved metal salts to their neutral states, leading them to aggregate into several-atom NCs [1,9]. However, stabilization is often a cause for great concern, and a proper stabilizing agent is required to protect each cluster from further aggregation into large nanoparticles [9].

A variety of protecting scaffolds have been used to stabilize NCs, from dendrimers, polymers, DNA, proteins, and peptides in the liquid phase [1,10,11] to glass, zeolite, and polymer in the solid state [12–14]. Solid-state matrices allow for the spatially controlled generation of localized NCs with high resolution, enabling compelling applications such as micro-labels in zeolite for anticounterfeiting applications [15] and optical memories in phosphate glasses [16]. NCs in these templates are fabricated using direct laser writing (DLW), where a tightly focused femtosecond laser beam is utilized to locally photo-reduce metal ions through a multi-photon absorption mechanism. These NCs are highly stable over extended periods and display bright fluorescence and excellent photostability. Nevertheless, in addition to the expensive high-intensity femtosecond

laser, the fabrication of NCs in these hosts suffers from the complexity of implementation and slow processing speed. For the case of phosphate glasses particularly, cumbersome sample preparation steps are also required.

In contrast, polymeric substrates provide suitable, cost-effective, and versatile alternatives to encapsulate NCs. Further, the required dose of exposure to generate NCs in the metal-precursor-containing polymer matrices is far smaller than that needed for the substrates mentioned above [17]. Despite the potential of polymer films for spatially controlled fabrication of fluorescent NCs, the synthesis of NCs in rigid polymer matrices using the DLW and light activation technique is currently limited to only a few polymers. Sakamoto *et al.* reported photofabrication of gold nanoclusters (AuNCs) in polyvinyl acetate (PVAc) films [18,19]. Recently, DLW of silver nanoclusters (AgNCs) and AuNCs in poly(methacrylic acid) (PMAA) and polyvinyl alcohol (PVA) thin films using femtosecond and continuous-wave (CW) lasers have also been reported [14,17,20–22]. These NCs manifest bright fluorescence and good photostability. Still, consideration of the new polymers could lead to the formation of NCs with unique properties, functionalities, and applications. Polycarbonate (PC) is an intriguing choice among many polymers available, owing to extreme toughness, durability, high heat distortion resistance, and excellent compatibility with other polymers. Also, PC is a highly transparent polymer with transmission to visible light superior to many glasses [23,24].

In this paper, we demonstrate the formation and stabilization of fluorescent AuNCs in PC films using a photochemical method. We study the optical properties and morphology of the fluorescent structures. The as-formed AuNCs are highly fluorescent and resistant to aging. We show the possibility of patterning arbitrary fluorescent markings in the film. These fluorescent markings reveal good photostability and could enable applications such as anticounterfeiting, security markings, and optical data storage.

## 2. Experimental

### 2.1. Film preparation

Polycarbonate granules (Goodfellow) were dissolved in chloroform (100 mg in 2 mL) and stirred for 30 min at room temperature. Next, depending on the targeted Au/PC weight ratio, a photoinitiator (Sigma-Aldrich, 2-Hydroxy-4'-(2-hydroxyethoxy)-2-methylpropiophenone, 0–9 mg) was added to the PC chloroform solution and stirred for another 10 min. A required amount of Gold(III) Chloride Trihydrate (Nanopartz,  $\text{HAuCl}_4 \cdot 3\text{H}_2\text{O}$ , >99.9%) was added to the solution to obtain the desired weight ratio of Au/PC (0–3%). A glass Petri dish was cleaned by 5 min ultrasonic bath of acetone and a rinse with isopropyl alcohol and distilled water; it was finally dried with nitrogen. The resulting solution was then dropcast in the glass Petri dish and heated at 60 °C until the solvent evaporation was complete. An extra 5 min heating at 80 °C was done to remove the residual solvent, leading to a dry composite film with a thickness of ~18  $\mu\text{m}$ .

### 2.2. Photoreduction

A light-emitting diode (LED) (Thorlabs, 365 nm, M365LP1) was collimated using an aspheric condenser lens (Thorlabs, 16 mm). A bandpass filter (Semrock, 370/36 nm) was used to avoid the LED spectrum overlapping the sample fluorescence, enabling in-situ monitoring of the fluorescence intensity evolution. Au@PC films were mounted on microscope slides and were exposed to the LED light. The intensity of the light impinging the film was set depending on the need. We used a collimated beam with an intensity of 180  $\text{mW}/\text{cm}^2$  to activate larger areas. However, for faster activations, a positive lens was used to focus the LED light into a small region, leading to an intensity of 1  $\text{W}/\text{cm}^2$ . The fluorescence evolution was concurrently imaged from the slide's backside using a CMOS camera (Thorlabs, DCC1545M) equipped with an emission filter (Semrock, BLP01-532R-25) and a lens system.

### 2.3. Optical characterization

Fluorescence emission and excitation spectra were measured using an FLS1000 Photoluminescence Spectrometer (Edinburgh Instruments). The absolute photoluminescence quantum yields (PLQYs) and the lifetime measurements were carried out using an FS5 Spectrofluorometer (Edinburgh Instruments). The PLQYs were assessed using an SC-30 module coupled with an Integrating Sphere with an excitation wavelength of 380 nm. The time-resolved photoluminescence (TRPL) decay was acquired and analyzed using a Time Correlation Single Photon Counting (TCSPC) system. A picosecond pulsed diode laser (EPL-375, Edinburgh Instruments) with a pulse width of 64.3 ps and wavelength of 377.6 nm was used to excite the samples.

### 2.4. Confocal fluorescence microscopy

The distribution of fluorescent NCs throughout the film thickness was studied by Zeiss LSM 800. The excitation laser wavelength was 405 nm. The fluorescence signal was collected by an oil-immersion objective (Plan-Apochromat 63×/1.4 Oil) in DAPI spectral range. False-color fluorescence images were plotted based on their raw values using Python.

### 2.5. Transmission electron microscopy (TEM)

TEM analysis was carried out using a JEM 2800 High resolution-TEM (JEOL Ltd) operated at 200 kV. To prepare the samples, Au@PC film containing fluorescent markings was first dissolved in chloroform. The as-obtained solution was then dropcast on copper grids that were coated with a holey carbon film.

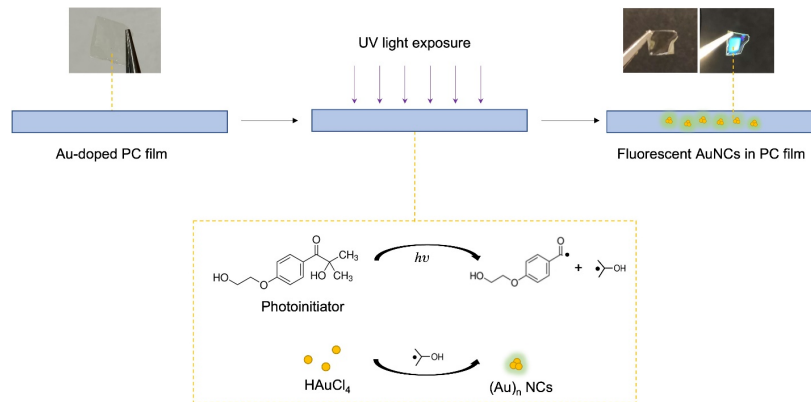
### 2.6. X-ray photoelectron spectroscopy (XPS)

XPS analysis was performed in Kratos Axis Ultra ESCA X-ray photoemission spectrometer, using Al K $\alpha$  radiation at E = 1486.69 eV. The operation pressure during the measurement was  $8 \times 10^{-8}$  Pa. The binding energy scale was referenced to 284.8 eV as determined by the location of the adventitious carbon peak in the C 1s spectra.

## 3. Results and discussion

A PC film doped with gold salt (the precursor for AuNCs) and photoinitiator (the source of electron donors) was first prepared. Both gold salt and photoinitiator were uniformly dispersed in the polymer to inhibit partial overconcentration, which would cause the formation of large particles after the photochemical reaction. The weight ratio of gold source to PC varied from 0 to 3%. The Au@PC film was colorless and transparent, with a thickness of about 18  $\mu\text{m}$ . Higher concentrations resulted in crystallization and opacity. Figure 1 illustrates the photosensitized reduction [25] and in-situ formation of AuNCs in an Au@PC film. Upon exposure to UV light, the photoinitiator produces active free radicals, which reduce Au(III) ions to Au(II) and Au(0) [26]. Then, absorption of the UV light raises the local temperature of the exposed area of the film, leading to the diffusion of Au(0) atoms and the formation of AuNCs [27]. The as-obtained AuNCs in PC film give out blue-green fluorescence when excited by a 365 nm light source. A more detailed understanding of the photophysical phenomena arising from Au@PC and UV light interaction is left for future work.

Figure 2(a) shows the UV-Vis absorption spectra of an Au@PC film (Au/PC of 2%) before and after exposure to UV light. After 30 min exposure to UV light with an intensity of 180 mW/cm<sup>2</sup>, the absorption at 300–380 nm reveals a notable drop due to the reduction of H<sub>2</sub>AuCl<sub>4</sub> ( $\lambda_{\text{max}}$  at 325 nm) and consumption of photoinitiator ( $\lambda_{\text{max}}$  at 274 nm). Nevertheless, the characteristic absorption at 500–550 nm for plasmonic AuNPs cannot be observed in the spectrum, ruling out the presence of larger AuNPs (see Fig. S1) [28,29]. This change in the absorption spectrum suggests the formation of gold entities (i.e., AuNCs) that are smaller than plasmonic AuNPs.



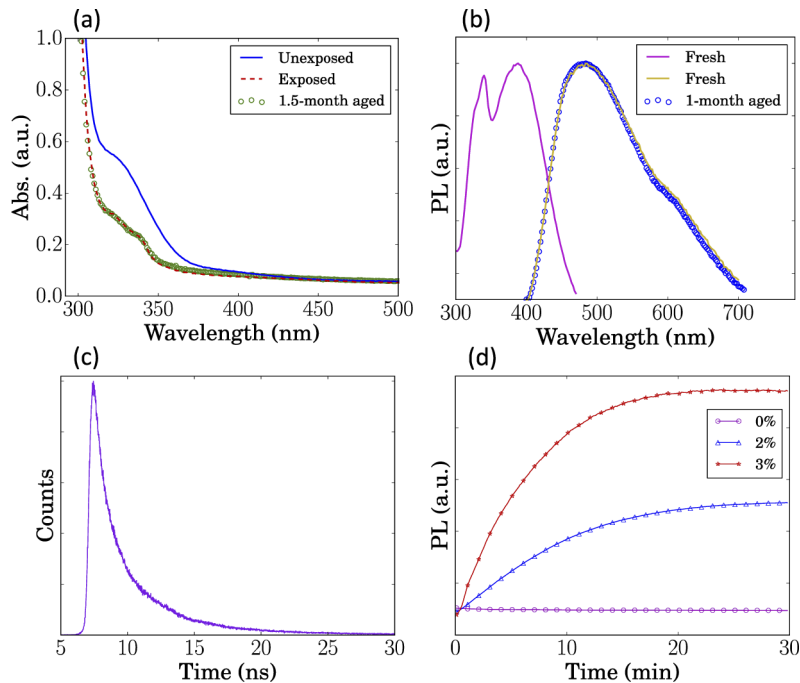
**Fig. 1.** In-situ generation of AuNCs in Au@PC film by UV light irradiation

Figure 2(b) shows the fluorescence excitation/emission of an Au@PC film (Au/PC of 3%) that was exposed for 5 min to UV light with an intensity of  $1 \text{ W/cm}^2$ . The excitation and emission spectra peak at 390 nm and 480 nm, respectively, corresponding to a Stokes shift of 90 nm. We find that the fluorescence is highly related to the gold particles, rather than PC or photoinitiator, in the composite film. Unexposed PC films doped with gold salt and photoinitiator and exposed PC films with no gold loadings with and without photoinitiator barely show any fluorescence, demonstrating the indispensable role of the gold element and the light irradiation (see Fig. S2).

The exposed film was stored in room condition for one month to assess the effect of aging. Neither the absorption nor the fluorescence of the Au@PC film has experienced changes during such period. As shown in Fig. 2(a), there is no observable shift in the absorbance spectrum after 6 weeks of storage, and the peak ascribed to plasmonic AuNPs remains absent, implying that the AuNPs formed within the film are scarce. This is further supported by the film retaining its transparent characteristics, confirming that the formation of larger gold particles is negligible. The emission spectrum after the long-time storage also verifies the stability of the AuNCs in the PC film (see Fig. 2(b)). The unchanged peak wavelength in the emission plots, which results in a fixed fluorescence color, suggests that the as-formed NCs do not tend to aggregate to form larger AuNCs emitting different colors. In fact, the PC matrix well confines the AuNCs from mobility and aggregation, thus exhibiting a superior anti-aging effect compared to a similar structure in a PVAc matrix [19]. It should be noted that fluorescence emission spectra in Fig. 2(b) are normalized since it was not practical to obtain identical alignments in fluorometer apparatus for measurements before and after aging. Still, the stability of the fluorescence intensity is studied using fluorescence microscopy and is discussed below.

Besides good storage stability, the AuNCs in PC film are highly fluorescent. Their absolute PLQYs were measured to be around 15%, remarkably higher than similar AuNCs in other polymers when no capping ligands are used [30]. Figure 2(c) exhibits the fluorescence decay curve of AuNCs generated in an Au@PC film, which determines the average fluorescence lifetime of 4.4 ns. The relatively short lifetime and Stokes shift (90 nm) suggest that the photoluminescence stems from the singlet intraband transitions within the metal core [31], rather than the charge transfer between the surface ligands and surface metal atoms [32].

The fluorescence intensity of AuNCs generated within Au@PC films depends on the intensity of the UV light source and the time of the exposure. While under-exposure could not reduce all gold ions in the film, over-exposure would lead to the formation of larger AuNPs that are not fluorescent. The non-optimal exposure results in fluorescent markings that do not have the



**Fig. 2.** (a) UV-Vis spectra of a 2% Au@PC film before and after exposure to UV light. The exposure was performed for 30 min with an intensity of  $180 \text{ mW/cm}^2$ . The spectrum of the film 1.5 months after the exposure is also shown. (b) Fluorescence emission and excitation spectra of a 3% Au@PC film exposed for 5 min to UV light with an intensity of  $1 \text{ W/cm}^2$ . The emission spectrum of the film after one month of storage is also plotted. (c) Fluorescence decay (at 512 nm) of a 3% Au@PC film that was exposed for 5 min to UV light with  $1 \text{ W/cm}^2$ . (d) Fluorescence intensity evolution of Au@PC films with different Au/PC ratios exposed to UV light with power set for  $180 \text{ mW/cm}^2$  intensity.

maximum possible brightness or are discolored due to the formation of NPs. Therefore, for better utilization of Au@PC films for fluorescent markings, it is crucial to investigate the time-dependence response of the fluorescence when exposed to UV light. Figure 2(d) illustrates the fluorescence intensity evolution of different Au@PC films that were exposed to UV light with an intensity of  $180 \text{ mW/cm}^2$ . While the film with no gold loading displays no fluorescence build-up, the fluorescence intensity of the films with gold additives grows with UV light irradiation. This growth further attests that the as-generated AuNCs give out the fluorescence emission. As seen, the process seems to be faster and brighter for higher gold loadings. Intuitively, in films with higher gold loading, reduced metal atoms are more likely to absorb one another, leading to a faster formation of AuNCs.

Interestingly, the as-generated AuNCs remain stable even when Au@PC film is fully dissolved in organic solvents (e.g., chloroform). As compared to the solid polymer matrix, there is much less steric confinement to inhibit aggregation. However, fluorescence from AuNCs still exists and can remain stable after dissolving a fluorescent Au@PC film in chloroform (see Fig. S3). This stability not only increases flexibility in practical applications but also enables direct observation of the micromorphology of AuNCs using TEM analysis. Figures 3(a) and (b) show the TEM image and EDX spectrum of the AuNCs in the Au@PC film chloroform solution. There are spherical particles with a size of  $1.68 \pm 0.51 \text{ nm}$ . These particles are mainly composed of Au elements (Cu comes from the TEM grids). In contrast to fluorescent films, over-exposed films

contained large AuNPs, and unexposed films show no AuNPs unless damaged by the electron beam in TEM (see Fig. S4).

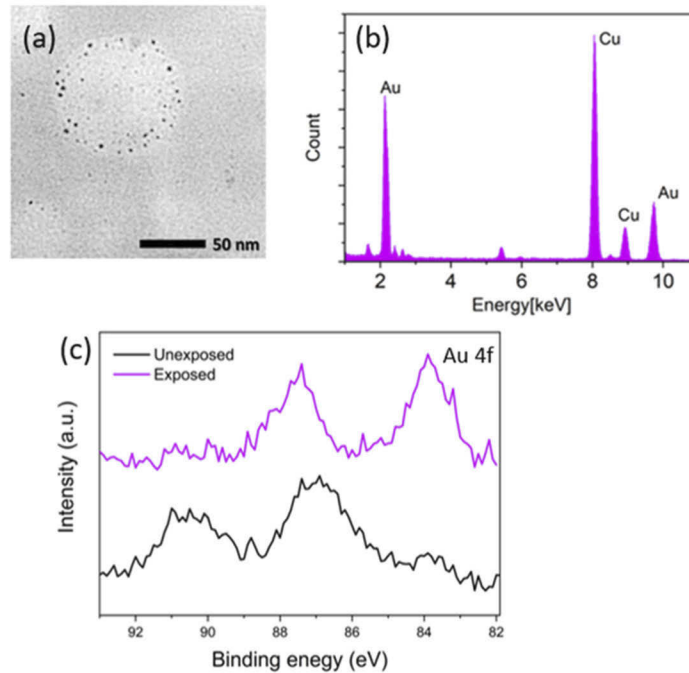


**Fig. 3.** Micromorphology and composition of the as-prepared AuNCs. (a) TEM image, and (b) EDX spectrum of the AuNCs in the film. Those ultra-small particles ( $\sim 1.68$  nm) are mainly composed of gold elements. (c) Binding energies of Au 4f in exposed (purple) and unexposed (black) Au@PC films. The difference in binding energies suggests Au(III) are reduced to Au(0) after exposure to UV light.

The valence state of Au in the fluorescent Au@PC film is investigated by XPS characterization (Fig. 3(c)). Binding energies of Au 4f in the Au@PC film exhibit a notable difference before and after UV light irradiation. In the unexposed film, the binding energies of Au  $4f_{7/2}$  and Au  $4f_{5/2}$  are 87.1 eV and 90.8 eV, respectively, which are assigned to Au(III) [33]. In contrast, in the exposed sample, Au  $4f_{7/2}$  and Au  $4f_{5/2}$  possess much lower binding energies of 83.8 eV and 87.6 eV, respectively, which are assigned to Au(0) [34]. Clearly, exposure to the high-intensity UV light has triggered a complete reduction of Au(III) ions in the film, giving rise to zero-valent gold nanoclusters. The full consumption of Au(III) ions was further confirmed by the binding energies remaining consistent after over-exposing the Au@PC film (see Fig. S5).

From the application point of view, knowledge about the spatial distribution of the AuNCs throughout the thickness of the PC film is crucial. To this end, confocal fluorescence imaging was performed on 3% Au@PC samples. Parts of the film were exposed for 30 min to UV light with intensity of  $180 \text{ mW/cm}^2$ . The exposed and unexposed regions of the film were examined by a laser scanning confocal fluorescence microscope with an excitation wavelength of 405 nm. The emission spectra were recorded in the DAPI spectral region. Fluorescence images were false-colored based on their intensity values using Python and are shown in Fig. 4 in XY and XZ planes. Compared to exposed areas, the fluorescence in the unexposed regions is negligible. The white dashed lines in Figs. 4(b) and (d) mark the edges of the fluorescence areas on the Z-axis in Fig. 4(d). This region corresponds to  $18 \mu\text{m}$  thickness, which is equal to the film thickness, confirming that the fluorescent features form throughout the film with no tendency towards any

parts. Therefore, it is impossible to remove the markings by scratching the surface of the film, as opposed to fluorescent inks, making it a reliable host to keep the markings protected against counterfeiters or harsh handling. It should be noted that more precise images could be obtained by deconvolution of the point spread function of the microscope objective and the film thickness. However, given the high NA of the objective (1.4) and the wavelength (405 nm) used for imaging, the axial resolution of the images is well below 1  $\mu\text{m}$ , enabling quite an accurate estimation of the film thickness according to the cross-sections of in XZ planes of the fluorescent images. Besides, considering the small absorbance at 405 nm, one can assume the excitation intensity was consistent throughout the film thickness.

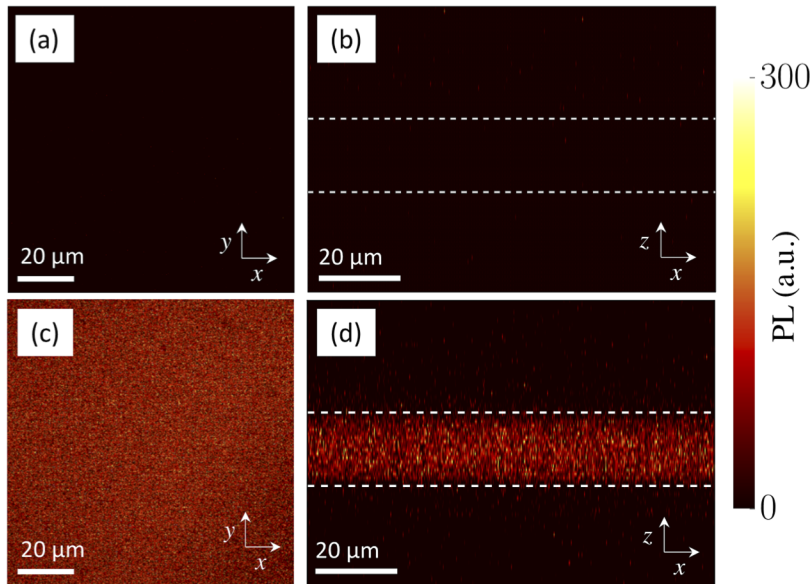


**Fig. 4.** Confocal fluorescence microscopy images of a 3% Au@PC film that was (a,b) unexposed and (c,d) exposed for 30 min to UV light intensity of 180 mW/cm<sup>2</sup>. (a,c) correspond to the central plane of the film in XY planes, and (b,d) are cross-sections in XZ planes. The white-dashed lines represent the approximate position of the film marked based on the edges of the fluorescent area in (d).

The light-induced processing of fluorescent NCs in Au@PC films enables spatially controlled photo-reduction of gold ions and the generation of permanent fluorescent patterns of arbitrary shapes. To demonstrate a proof-of-principle of the light patterning technique, we exposed a 3% Au@PC film through a photomask to UV light with an intensity of 1 W/cm<sup>2</sup>. As discussed above, the exposure was stopped after 5 minutes elapsed to ensure reaching maximum fluorescence intensity and having minimum bleaching. Figure 5(a) shows a false-color fluorescence microscopy image of a flower made using the photomask. As can be seen, detailed fluorescent markings can be made in areas as small as 1 mm<sup>2</sup>. Here, the resolution is determined by the photomask. However, the minimum fluorescent feature size ( $d$ ) that can be made in Au@PC films is limited by the diffraction of light and is given by  $d = 0.61\lambda/\text{NA}$  [35], where  $\lambda$  is the wavelength of the light source used for photofabrication, and NA is the numerical aperture of the lens focusing the light onto the film. Therefore, in principle, it is possible to pattern fluorescent markings with resolution beyond micrometer scale [17], which outperforms fluorescent inks with spatial resolution in the range of 100–500  $\mu\text{m}$  [36]. Furthermore, the light intensity used to activate fluorescent AuNCs in PC films is several orders of magnitude lower than that needed in other solid-state matrices like glass [27], where a complex optical setup and expensive femtosecond

laser are required. In fact, the low-intensity requirement for activation of NCs in Au@PC film enables the parallel patterning through the photomask without the need for the typical scanning approach of the DLW technique. Clearly, using a light source with appropriately high power, the parallel patterning can be done in a much shorter time scale. Thus, the proposed material system allows low-cost and straightforward photofabrication of fluorescent markings that can be used as authenticity markings for important documents and valuable products.

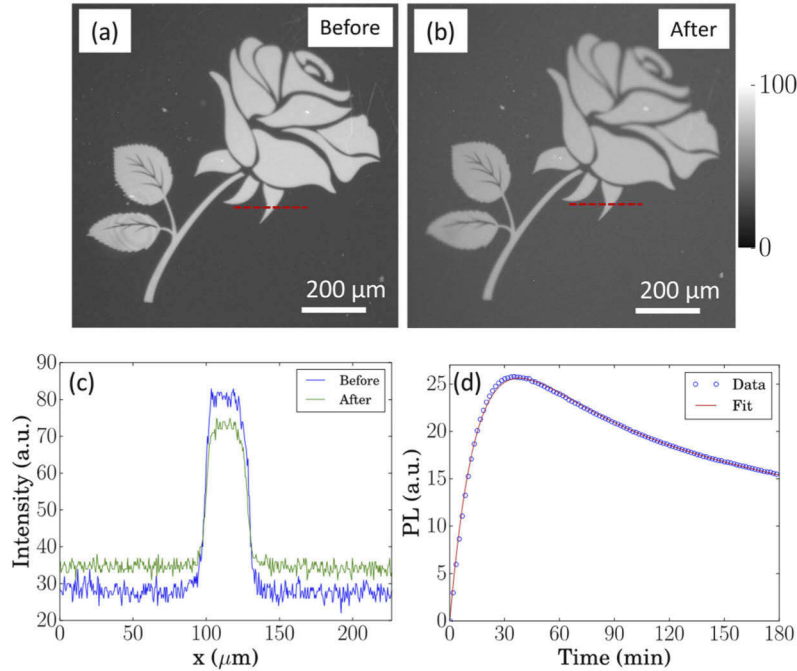


**Fig. 5.** (a,b) False-color fluorescence microscopy images of a pattern (a) before and (b) after 6-hour exposure to UV light of a banknote scanner with an intensity of  $3.5 \text{ mW/cm}^2$ . The patterns were made by 5-min exposure of the Au@PC film through a photomask with an intensity of  $1 \text{ W/cm}^2$ . (c) Intensity profiles of single-pixel values along the red dashed lines in (a) and (b). (d) Fluorescence intensity evolution of a 3% Au@PC film exposed to 365 nm LED with an intensity of  $180 \text{ mW/cm}^2$ .

Fluorescent markings in security applications should survive numerous readings without fading out. Here, the fade-out can occur either due to the bleaching of the fluorescent patterns or the activation of fluorescent NCs in the background. To study the effect of the reading, the fluorescent markings shown in Fig. 5(a) were placed under a UV banknote scanner (Safescan 50, 365 nm) for 6 hours. The intensity of the scanner was estimated to be around  $3.5 \text{ mW/cm}^2$ . Figure 5(b) shows a false-color fluorescence microscopy image of the flower pattern after exposure to the banknote scanner. Figure 5(c) illustrates the intensity profiles along the red dashed lines in Figs. 5(a) and (b). From these profiles, one can estimate that the contrast of the markings has declined from 48% to 35% after the 6-hour reading. The reduction in the contrast arises both from the activation of AuNCs in the background regions and from the decay of the fluorescence of the patterns. Despite this, the fluorescent codes were still clear and readable.

The photostability of AuNCs in PC film is further investigated by prolonged exposure and in-situ recordings of fluorescence intensity evolution. We used a 3% Au@PC film and exposed it for 180 min to an intensity of  $180 \text{ mW/cm}^2$ , which is the intensity used to generate AuNCs. This level of intensity is significantly higher than the intensity of typical UV scanners used to detect

fluorescent markings. Figure 5(d) shows the evolution of the fluorescence intensity pertaining to prolonged exposure. While the growing part of the curve is related to the consumption of gold ions and the production of AuNCs, the decline can be mainly attributed to the transformation of AuNCs into larger non-fluorescent AuNPs—there might also be other mechanisms involved in the bleaching of fluorescence, which will be studied in future work. A single exponential term with a time constant of  $\tau_1$  can well describe the rising part of the fluorescence curve. In contrast, the decaying part exhibits fast and slow decay components, corresponding to two time constants of  $\tau_2$  and  $\tau_3$ . Similar two-term exponential decay is previously reported for fluorescence bleaching of silver nanoclusters in polymer films [14]. The dynamics of the in-situ production and bleaching of fluorescent AuNCs can be modelled with a function  $y(t) = a_0 (-\exp(-t/\tau_1) + b_0 \exp(-t/\tau_2) + (1 - b_0) \exp(-t/\tau_3))$ , where  $a_0$  and  $b_0$  are amplitude parameters. Figure 5(d) shows an excellent fit between the model and the fluorescence evolution data with a coefficient of determination of  $R^2 \sim 0.997$  using  $\tau_1 \sim 16$  min,  $\tau_2 \sim 40$  min, and  $\tau_3 \sim 428$  min. According to these time constants, part of the as-formed AuNCs grows to AuNPs with a fast rate being still 2.5 times slower than the AuNCs formation rate. The other part of the fluorescence decays  $\sim 10$  times slower than the fast rate, making the fluorescence stable for a significantly extended time. The rise and decay time constants are intensity-dependent: the higher the intensity used to irradiate Au@PC film, the faster the rate at which the fluorescence intensity develops and fades out. Similar behavior was also shown for AuNCs in PVA films [17]. Considering that the reading of the as-fabricated fluorescent markings is typically done using a significantly lower intensity ( $\sim 3\text{--}6$  mW/cm<sup>2</sup>) than what used here to generate AuNCs, one can conclude that the AuNCs developed in PC films are highly photostable and could maintain the fluorescence for a long period, enabling reading of thousands of times without being fade out.

#### 4. Conclusion

We demonstrated that polycarbonate, an essential polymer for industrial applications, can be used as a flexible matrix for in-situ photofabrication of fluorescent AuNCs. The fabrication can be made using a low-cost LED and requires remarkably lower light intensity than those made in other rigid templates like glass and zeolite. The low required dose of light for activation of AuNCs in PC film enables the parallel light patterning of fluorescent markings, eliminating the need for slow point-by-point scanning and cumbersome implementation of the DLW technique. The AuNCs made in PC film are stable and can withstand several hours of reading by standard UV scanners. In addition, the emission spectral shape of these NCs does not change by aging, and their fluorescence color remains consistent. Besides, the markings are made through the whole film thickness and cannot be scratched away from the surface. The proposed bright and photostable features could find various applications, for example, in anti-counterfeiting and security markings.

**Funding.** Academy of Finland (310799, 320165, 326409).

**Acknowledgments.** This work made use of Tampere Imaging Facility (TIF) and Tampere Microscopy Center facilities at Tampere University and Nanomicroscopy Center (Aalto-NMC) at Aalto University.

**Disclosures.** The authors declare no competing financial interest.

**Data availability.** Data underlying the results presented in this paper are not publicly available at this time but may be obtained from the authors upon reasonable request.

**Supplemental document.** See [Supplement 1](#) for supporting content.

#### References

1. I. Diez and R. H. A. Ras, "Fluorescent silver nanoclusters," *Nanoscale* **3**(5), 1963–1970 (2011).
2. Y. Lu and W. Chen, "Sub-nanometre sized metal clusters: from synthetic challenges to the unique property discoveries," *Chem. Soc. Rev.* **41**(9), 3594–3623 (2012).
3. A. Cantelli, G. Guidetti, J. Manzi, V. Caponetti, and M. Montalti, "Towards ultra-bright gold nanoclusters," *Eur. J. Inorg. Chem.* **2017**(44), 5068–5084 (2017).

4. J. Zheng, P. R. Nicovich, and R. M. Dickson, "Highly fluorescent noble-metal quantum dots," *Annu. Rev. Phys. Chem.* **58**(1), 409–431 (2007).
5. L. Shang, S. Dong, and G. U. Nienhaus, "Ultra-small fluorescent metal nanoclusters: Synthesis and biological applications," *Nano Today* **6**(4), 401–418 (2011).
6. L. Zhang and E. Wang, "Metal nanoclusters: New fluorescent probes for sensors and bioimaging," *Nano Today* **9**(1), 132–157 (2014).
7. G. Ou, J. Zhao, P. Chen, C. Xiong, F. Dong, B. Li, and X. Feng, "Fabrication and application of noble metal nanoclusters as optical sensors for toxic metal ions," *Anal Bioanal Chem* **410**(10), 2485–2498 (2018).
8. L.-Y. Chen, C.-W. Wang, Z. Yuan, and H.-T. Chang, "Fluorescent gold nanoclusters: recent advances in sensing and imaging," *Anal. Chem.* **87**(1), 216–229 (2015).
9. R. Jin, "Quantum sized, thiolate-protected gold nanoclusters," *Nanoscale* **2**(3), 343–362 (2010).
10. T. Vosch, Y. Antoku, J.-C. Hsiang, C. I. Richards, J. I. Gonzalez, and R. M. Dickson, "Strongly emissive individual DNA-encapsulated Ag nanoclusters as single-molecule fluorophores," *Proc. Natl. Acad. Sci.* **104**(31), 12616–12621 (2007).
11. R. Jin, "Atomically precise metal nanoclusters: stable sizes and optical properties," *Nanoscale* **7**(5), 1549–1565 (2015).
12. C. Maurel, T. Cardinal, M. Bellec, L. Canioni, B. Bousquet, M. Treguer, J. J. Videau, J. Choi, and M. Richardson, "Luminescence properties of silver zinc phosphate glasses following different irradiations," *J. Lumin.* **129**(12), 1514–1518 (2009).
13. G. De'Cremer, Y. Antoku, M. B. J. Roefsaers, M. Sliwa, J. Van Noyen, S. Smout, J. Hofkens, D. E. De Vos, B. F. Sels, and T. Vosch, "Photoactivation of Silver-Exchanged Zeolite A," *Angew. Chem. Int. Ed.* **47**(15), 2813–2816 (2008).
14. P. Kunwar, J. Hassinen, G. Bautista, R. H. A. Ras, and J. Toivonen, "Direct laser writing of photostable fluorescent silver nanoclusters in polymer films," *ACS Nano* **8**(11), 11165–11171 (2014).
15. G. De Cremer, B. F. Sels, J. Hotta, M. B. J. Roefsaers, E. Bartholomeeusen, E. Coutiño-Gonzalez, V. Valtchev, D. E. De Vos, T. Vosch, and J. Hofkens, "Optical Encoding of Silver Zeolite Microcarriers," *Adv. Mater.* **22**(9), 957–960 (2010).
16. A. Royon, K. Bourhis, M. Bellec, G. Papon, B. Bousquet, Y. Deshayes, T. Cardinal, and L. Canioni, "Silver Clusters Embedded in Glass as a Perennial High Capacity Optical Recording Medium," *Adv. Mater.* **22**(46), 5282–5286 (2010).
17. M. H. Bitarafan, S. Suomala, and J. Toivonen, "Sub-microwatt direct laser writing of fluorescent gold nanoclusters in polymer films," *Opt. Mater. Express* **10**(1), 138–148 (2020).
18. M. Sakamoto, T. Tachikawa, M. Fujitsuka, and T. Majima, "Photoreactivity of As-Fabricated Au Clusters at the Single-Cluster Level," *J. Am. Chem. Soc.* **131**(1), 6–7 (2009).
19. M. Sakamoto, T. Tachikawa, M. Fujitsuka, and T. Majima, "Photochemical Reactivity of Gold Clusters: Dependence on Size and Spin Multiplicity  $\uparrow$ ," *Langmuir* **25**(24), 13888–13893 (2009).
20. P. Kunwar, J. Hassinen, G. Bautista, R. H. A. Ras, and J. Toivonen, "Sub-micron scale patterning of fluorescent silver nanoclusters using low-power laser," *Sci Rep* **6**(1), 23998 (2016).
21. N. Karimi, P. Kunwar, J. Hassinen, R. H. A. Ras, and J. Toivonen, "Micropatterning of silver nanoclusters embedded in polyvinyl alcohol films," *Opt. Lett.* **41**(15), 3627–3630 (2016).
22. L. E. Mulko, M. Rossa, J. P. Aranguren-Abrate, and G. A. Pino, "Micropatterning of fluorescent silver nanoclusters in polymer films by Laser Interference," *Appl. Surf. Sci.* **485**, 141–146 (2019).
23. V. C. Rucker, K. L. Havenstrite, B. A. Simmons, S. M. Sickafoose, A. E. Herr, and R. Shediach, "Functional Antibody Immobilization on 3-Dimensional Polymeric Surfaces Generated by Reactive Ion Etching," *Langmuir* **21**(17), 7621–7625 (2005).
24. K. Aslan, P. Holley, and C. D. Geddes, "Metal-enhanced fluorescence from silver nanoparticle-deposited polycarbonate substrates," *J. Mater. Chem.* **16**(27), 2846–2852 (2006).
25. M. Sakamoto, M. Fujitsuka, and T. Majima, "Light as a construction tool of metal nanoparticles: Synthesis and mechanism," *Journal of Photochemistry and Photobiology C: Photochemistry Reviews* **10**(1), 33–56 (2009).
26. M. L. Marin, K. L. McGilvray, and J. C. Scaiano, "Photochemical strategies for the synthesis of gold nanoparticles from Au(III) and Au(I) using photoinduced free radical generation," *J. Am. Chem. Soc.* **130**(49), 16572–16584 (2008).
27. M. Bellec, A. Royon, B. Bousquet, K. Bourhis, M. Treguer, T. Cardinal, M. Richardson, and L. Canioni, "Beat the diffraction limit in 3D direct laser writing in photosensitive glass," *Opt. Express* **17**(12), 10304–10318 (2009).
28. E. Nadal, N. Barros, H. Glénat, J. Laverdant, D. S. Schmool, and H. Kachkachi, "Plasmon-enhanced diffraction in nanoparticle gratings fabricated by in situ photo-reduction of gold chloride doped polymer thin films by laser interference patterning," *J. Mater. Chem. C* **5**(14), 3553–3560 (2017).
29. M. H. Bitarafan, S. Annurakshita, J. Toivonen, and G. Bautista, "Maskless fabrication of plasmonic metasurfaces in polymer film using a spatial light modulator," *Opt. Lett.* **46**(6), 1197–1200 (2021).
30. U. Divya Madhuri and T. P. Radhakrishnan, "Gold nanoclusters with a wide range of fluorescence characteristics generated in situ in polymer thin films: potential gas sensing application," *Dalton Trans.* **46**(46), 16236–16243 (2017).
31. J. Zheng, C. Zhang, and R. M. Dickson, "Highly Fluorescent, water-soluble, size-tunable gold quantum dots," *Phys. Rev. Lett.* **93**(7), 077402 (2004).

32. K. Pyo, V. D. Thanthirige, K. Kwak, P. Pandurangan, G. Ramakrishna, and D. Lee, "Ultrabright Luminescence from Gold Nanoclusters: Rigidifying the Au(I)-Thiolate Shell," *J. Am. Chem. Soc.* **137**(25), 8244–8250 (2015).
33. F. Zhu, L. Peng, X. Yao, Y. Zhang, C. Zhang, and X. Gu, "Hollow-fiber-supported gold and zirconium-doped faujasite catalytic membranes for hydrogen purification," *Energy Technol.* **5**(12), 2283–2293 (2017).
34. L. Li, Z. Li, H. Zhang, S. Zhang, I. Majeed, and B. Tan, "Effect of polymer ligand structures on fluorescence of gold clusters prepared by photoreduction," *Nanoscale* **5**(5), 1986–1992 (2013).
35. E. Hecht, *Optics* (Pearson, 2017), Chap 10.
36. M. You, J. Zhong, Y. Hong, Z. Duan, M. Lin, and F. Xu, "Inkjet printing of upconversion nanoparticles for anti-counterfeit applications," *Nanoscale* **7**(10), 4423–4431 (2015).